

## The effects of different parameter regimes in geodynamo simulations

DARCY E. OGDEN\*, GARY A. GLATZMAIER and ROBERT S. COE

Earth Sciences Department, University of California, Santa Cruz, California 95064, USA

(Received 31 August 2005; in final form 13 March 2006)

Over the past 10 years, geodynamo simulations have grown rapidly in sophistication. However, it is still necessary to make certain approximations in order to maintain numerical stability. In addition, models are forced to make assumptions about poorly known parameters for the Earth's core. Different magnetic Prandtl numbers have been used and different assumptions about the presence of radiogenic heating have been made. This study examines some of the consequences of different approximations and assumptions using the Glatzmaier–Roberts geodynamo model. Here, we show that the choice of magnetic Prandtl number has a greater influence on the character of the magnetic field produced than the addition of a plausible amount of radiogenic heating. In particular, we find that prescribing a magnetic Prandtl number of unity with Ekman number limited by current computing resources, results in magnetic fields with significantly smaller intensities and variabilities compared with the much more Earth-like results obtained from simulations with large magnetic Prandtl numbers. A magnetic Prandtl number of unity, with both the viscous and magnetic diffusivities set to the Earth's magnetic diffusivity, requires a rotation rate much smaller than that of the Earth for currently reachable Ekman numbers. This results in a reduced dominance of the Coriolis forces relative to the buoyancy forces, and therefore, a reduction in the magnetic field intensity and the variability compared to the large Prandtl number cases.

*Keywords:* Geodynamo simulations; Magnetic Prandtl number; Radiogenic heating

### 1. Introduction

Over the past decade, a number of fully nonlinear, three-dimensional numerical simulations of the geodynamo have been published. Several reviews describe and compare these simulations (e.g. Glatzmaier and Roberts 1997, Fearn 1998, Busse 2000, Roberts and Glatzmaier 2000, Dormy *et al.* 2000, Christensen *et al.* 2001, Busse 2002, Kono and Roberts 2002, Glatzmaier 2002). However, no computer simulation of the geodynamo has yet been run in a realistic parameter regime. Due to the current limitations in computational resources, it is necessary to make approximations.

---

\*Corresponding author. Email: dogden@es.ucsc.edu

Although geodynamo simulations have been time dependent and chaotic, none has reached the strong turbulence expected in the Earth's fluid core.

Typically, the geodynamo simulations have fallen into two categories. Some simulations use the correct rotation rate and magnetic diffusivity and a realistic estimate of the core mantle boundary (CMB) heat flux. For these geodynamo models, the viscosity, which should be much less than the magnetic diffusivity, needs to be set about three orders of magnitude larger than the Earth's actual magnetic diffusivity. This is because the numerical resolution constrains the value of the Ekman number to maintain the numerical stability. This method has been adopted in all previous studies using the Glatzmaier–Roberts geodynamo model. A more common choice has been to set the viscous diffusivity equal to the magnetic diffusivity, which forces the rotation rate to be set several orders of magnitude smaller than that of the Earth in order to maintain numerical stability. To test the impact of these different choices, the present study compares the simulations of both types using the Glatzmaier–Roberts geodynamo model.

In addition to making these numerical approximations, geodynamo simulations are required to make assumptions about some properties of the Earth's core. One of these assumptions is about the radiogenic heating in the Earth's fluid outer core (FOC). For the past 25 years, it has generally been accepted that there are no radiogenic elements in the FOC (Stacey 1992). However, the past 10 years have seen new geochemistry studies suggesting that potassium might have partitioned into the core, during formation (Parker *et al.* 1996, Ohtani *et al.* 1997, Chabot and Drake 1999, Gessman and Wood 2002, Murthy *et al.* 2003), and more sophisticated thermal evolution models have been developed that require the presence of radioactive heating in the core (Buffett 2002, Brodholt and Nimmo 2002, Nimmo *et al.* 2004). Since the geodynamo is powered by convection, assumptions about the distribution of the heat source driving convection may be important to the character of the dynamo produced. Most geodynamo simulations have assumed no radiogenic heating the core. This study examines the effects of a plausible amount of core radiogenic heating in geodynamo simulations.

## 2. Numerical model

The Glatzmaier–Roberts geodynamo model is a three-dimensional spherical magnetohydrodynamics computer code that runs on massively parallel computers. This nonlinear model solves for the time and spatially dependent thermodynamic, velocity, and magnetic fields. The model is based on the anelastic equations of motion, which allow for radially dependent background thermodynamic variables. All other geodynamo models, other than the fully compressible model of Kageyama and Sato (1995), employ the Boussinesq approximation, which assumes the background density to be independent of radius. (For a detailed description of the model, see Glatzmaier 1984 and Glatzmaier and Roberts 1996a). For this study, we compare five different cases performed with the Glatzmaier–Roberts geodynamo model (table 1). The results from two of these simulations (cases 3 and 4) have been reported previously (Glatzmaier *et al.* 1999) and three are reported for the first time in this study.

Cases 3, 4, and 5 are run in the same basic parameter regime as all other previous studies with the Glatzmaier–Roberts model. They use the Earth values for the rotation

rate and CMB heat flux. In these cases, the magnetic ( $\eta$ ), thermal ( $\kappa$ ), and compositional diffusivities are set to the Earth's actual magnetic diffusivity ( $2 \text{ m}^2\text{s}^{-1}$ ); but, because of computational limitations, turbulent viscous diffusivity ( $\nu$ ) is set to  $1420 \text{ m}^2\text{s}^{-1}$  for cases 3 and 4, and  $2000 \text{ m}^2\text{s}^{-1}$  for case 5 (i.e., much larger than it should be). Cases 3 and 4 are discussed in more detail as cases 'g' and 'h', respectively, in Glatzmaier *et al.* (1999). For cases 3–5 the Coriolis force is treated implicitly and the nonaxisymmetric Reynolds stress terms are neglected. These cases also include hyperdiffusion, which is a numerical technique that allows less diffusion on the large global scales of momentum, entropy, composition, and magnetic field while providing sufficient diffusion at the smallest scales to prevent the buildup of the cascading energy. Cases 3 and 4 use a hyperdiffusion that increases as the spherical harmonic degree is cubed, with diffusivities at degree 21 being 350 times greater than that at degree 1. Case 5 uses a small amount of hyperdiffusion; diffusivities increase as the square of the degree and are 20 times greater at degree 95 compared to their minimum values at degree 1. See table 1 for more details regarding non-dimensional parameters, spatial resolution and numerical methods table 2 for definitions of symbols used here, and table 3 for definitions of non-dimensional numbers.

Cases 1 and 2 are in a new parameter regime compared with the previously published studies with the Glatzmaier–Roberts model. Internal heating equivalent to about 250 ppm of potassium in the Earth's core is added to the model FOC in case 2. In addition, both of these new simulations use higher spatial resolution – 144 grid points in latitude and longitude and 145 grid points in radius (approximately 100 km resolution in the horizontal direction and 10 km in the vertical direction) and a rhomboidal, instead of a triangular, truncation of spherical harmonics is used. The full nonlinear Reynolds stress terms in the momentum equation are retained and

Table 1. Simulated cases compared in this study. Cases 3 and 4 are cases 'g' and 'h', respectively, from Glatzmaier *et al.* (1999). Cases 1, 2, and 5 have not been previously published. (\*) denotes the strongly time, dependent diagnostic numbers for which a typical value for the simulation has been listed. These numbers do not account for the effects of hyperdiffusion in cases 3 and 4.

Case	1	2	3	4	5
$Ra$	$1.4 \times 10^8$	$1.4 \times 10^8$	$1.4 \times 10^9$	$1.4 \times 10^9$	$1.0 \times 10^9$
$Pr$	1	1	725	725	1000
$P_m$	1	1	725	725	1000
$q$	1	1	1	1	1
$E_k$	$1.3 \times 10^{-5}$	$1.3 \times 10^{-5}$	$2.0 \times 10^{-6}$	$2.0 \times 10^{-6}$	$2.7 \times 10^{-6}$
$\Delta \bar{E}^*$	100	100	100	100	400
$R_m^*$	1000	1000	2000	2000	6000
$Ro_c$	$5.36 \times 10^{-2}$	$5.03 \times 10^{-2}$	$2.0 \times 10^{-3}$	$2.0 \times 10^{-3}$	$2.7 \times 10^{-3}$
Radial levels in FOC	145	145	49	49	49
Radial levels in SIC	17	17	17	17	17
Longitudinal levels	144	144	64	64	144
Latitudinal levels	144	144	32	32	144
Spherical harmonic truncation	Rhomboidal	Rhomboidal	Triangular	Triangular	Rhomboidal
Coriolis terms	Explicit	Explicit	Implicit	Implicit	Implicit
Boundary condition	Tomographic	Tomographic	Homogeneous	Tomographic	Homogeneous
Nonaxisymmetrical Reynolds stress	Yes	Yes	No	No	No
Internal heating	No	Yes	No	No	No
Hyperdiffusion	No	No	Yes	Yes	Small

Table 2. Symbols used.

Symbol	Definition
$D$	Depth of the Earth's outer core
$S$	Entropy
$\rho$	Density
$r$	Radius
$\kappa$	Thermal diffusivity
$\nu$	Turbulent viscous diffusivity
$g$	Gravitational acceleration
$\eta$	Magnetic diffusivity
$\Omega$	Mean rotation rate of model planet
$B$	Magnetic field amplitude
$\mu$	Dynamic viscosity = $\rho\nu$
$v$	Velocity

Table 3. Non-dimensional numbers.

Symbol	Definition
$Ra = \left( \frac{gD^4(\partial\rho/\partial S)(dS/dr)}{\rho\nu\kappa} \right)_{CMB}$	Rayleigh number
$Pr = \nu\kappa^{-1}$	Prandtl number
$P_m = \nu\eta^{-1}$	Magnetic Prandtl number
$E_k = \nu(2\Omega D^2)^{-1}$	Ekman number
$Ro_c = E_k \left( \frac{Ra}{Pr} \right)^{1/2}$	Convective Rossby number
$\Lambda_E = (B_{\max}^2)(2\Omega\mu\rho\eta)^{-1}$	Elsasser number
$R_m = (v_{\max}D)\eta^{-1}$	Magnetic Reynolds number
$q = \kappa\eta^{-1}$	Roberts number

there is no hyperdiffusion. We set all our diffusivities, including the viscous diffusivity, to  $2\text{ m}^2\text{ s}^{-1}$ . All Prandtl numbers are therefore equal to 1 (see tables 2 and 3). The Ekman number ( $E_k = \nu(2\Omega D^2)^{-1}$ ) is set to  $1.3 \times 10^{-5}$ . The smallness of this value is limited by the spatial resolution we have chosen and the lack of hyperdiffusion. Consequently, because of the much smaller  $\nu$ , the rotation rate for this model ( $1.5 \times 10^{-8}\text{ s}^{-1}$ ) must be set much smaller than that of the Earth ( $7.29 \times 10^{-5}\text{ s}^{-1}$ ). Likewise, to maintain the numerically stable convection with this lower viscosity, we must limit the Rayleigh number ( $Ra$ ) by prescribing a much smaller superadiabatic heat flow through the CMB ( $3 \times 10^8\text{ W}$ ) than that of cases 3–5 and previous Glatzmaier–Roberts simulations (about  $2 \times 10^{12}\text{ W}$ ). The superadiabatic heat flow is chosen to produce convective velocities within the model core that are of the same order of magnitude as what is expected for the Earth's FOC.

There are many ways to define the Rayleigh number. Since there is no compositional flux through the CMB in these cases and we prescribe the heat flux at the CMB via the radial entropy gradient, we choose the following definition for the Rayleigh number:  $Ra = (gD^4(\partial\rho/\partial S)(dS/dr)(\rho\nu\kappa)^{-1})_{CMB}$ . The values of  $Ra$  for the five cases are listed in table 3; they are roughly between 10 and 20 times the critical  $Ra$ .

The choice of parameters for cases 1 and 2 is roughly the way most other geodynamo models have been set up. Unfortunately, neither choice, the large Prandtl number ( $Pr$ ) of cases 3–5 or the small rotation rate of cases 1 and 2 is satisfactory (Glatzmaier 2002);

more realistic simulations will require more computational resources and improved numerical methods.

The same thermal and compositional boundary conditions at the inner core boundary (ICB) are used for all five cases. As described in Glatzmaier and Roberts (1996a), the local heat flux, compositional flux, temperature, composition, and entropy all vary with time and location on the ICB. The boundary condition is that the latent heat flux (via the radial entropy gradient) and the compositional flux (via the radial compositional gradient) are constrained to be proportional to the cooling and growth rates at all times and the locations on the solid inner core boundary. The constants of proportionality are based on the best estimates of the material properties of the core. The buoyancy flux due to composition is prescribed to be 3 times greater than that due to entropy for all cases here. Consequently, the convection and the magnetic field in the core are driven by the prescribed heat flux at the CMB; the compositional flux is set to zero at the CMB. Cases 1, 2, and 4 have a tomographic heat flux pattern imposed at the CMB (Glatzmaier *et al.* 1999). The pattern is defined up to spherical harmonic degree and order four and ranges from zero heat flux to twice the mean CMB heat flux value. The other cases have uniform heat flux prescribed on the CMB. The effects of different CMB heat flux conditions on geodynamo simulations are explored in Glatzmaier *et al.* (1999).

For case 2, we prescribe the amount of radiogenic heating to be proportional to density, and therefore a function of radius. We set the total radiogenic heating to be 25% of the model's superadiabatic heat flow at the CMB. This amount of potassium is consistent with the reliable estimates based on the experimental data (Gessman and Wood 2002, Murthy *et al.* 2003). The same superadiabatic heat flow through the CMB is prescribed for cases 1 and 2, however, this heat flow is less than that used for previous Glatzmaier–Roberts simulations because, as discussed above, of the much smaller viscosity used here.

Cases 3 and 4 use 32 grid points in latitude and 64 in longitude for each radial level. These two cases employ a triangular truncation of the spherical harmonics in the spectral expansions of the horizontal dependencies of all variables. That is, all degrees ( $l$ ) up to a maximum ( $l_{max}$ ) and all orders for these degrees (longitudinal wavenumbers,  $|m| \leq l$ ) are included in the expansions. This means that a spherical harmonic with high resolution in longitude has low resolution in latitude, and vice versa. For these cases,  $l_{max}$  (and therefore also  $m_{max}$ ) is 21 which requires 64 longitudinal grid points and 32 latitudinal grid points, for every radial level to maintain alias-free nonlinear terms. The lower spatial resolution and greater hyperdiffusion of cases 3 and 4 obviously result in a greater fraction of the energy in the large global scales. Case 5 uses the same radial resolution as cases 3 and 4, but has the same horizontal resolution as cases 1 and 2.

Rhomboidal truncation of spherical harmonics is used in cases 1, 2 and 5. That is, ( $0 \leq |m| \leq m_{max}$ ) and ( $|m| \leq l \leq |m| + l_{max_0}$ ). Therefore, the minimum  $|m|$  for a given  $l$  is not necessarily 0:  $m_{min} = \max(0, l - m_{max})$ . This provides the same number of degrees ( $l$ ) for each order ( $m$ ). Therefore, the resolution in latitude is independent of the resolution in longitude, which some argue to be important for rapidly rotating systems. For the three cases here that use rhomboidal truncation,  $l_{max_0} = 48$ ,  $m_{max} = 47$  and therefore, for  $m = m_{max}$ ,  $l = 95$ . Alias-free nonlinear products with this spherical harmonic truncation require 144 grid points in both longitude and latitude for each radial level.

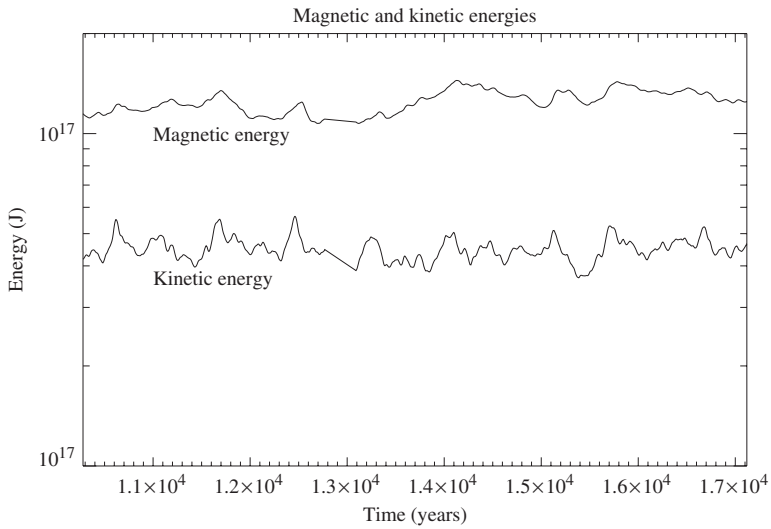


Figure 1. Average magnetic and kinetic energies of case 1 over time. A section of the simulation here shows statistically steady energies typical of cases 1 and 2.

The radial dependency is also spectral, involving an expansion in Chebyshev polynomials. In grid space, the Chebyshev levels are naturally more concentrated near the boundaries, which provides greater resolution in the viscous and thermal boundary layers where it is usually needed. Cases 3–5 have 49 Chebyshev levels in the outer core; the other cases have 145 Chebyshev levels. In addition, all cases use 17 levels in a half-Chebyshev space within the inner core to solve for the magnetic field.

The low resolution cases (3 and 4), which treat the Coriolis forces implicitly, can be run with a larger numerical time step (15 days) and for many more steps (10,000,000) to span several hundred thousand years. Case 5 uses a time step of 1.7 days for about 500,000 steps to span about 2000 years (starting from case 3); only the last 1000 years are used here. Note that time in these three cases correctly represent both the rotation period (1 day) and the magnetic dipole diffusion time (20,000 years). Cases 1 and 2 typically use a 7-day time step for about 1,500,000 steps and so span about 30,000 years, based on a 20,000-year magnetic dipole diffusion time. However, as is the case for all other geodynamo models that use a Prandtl number of unity, the time span for cases 1 and 2 is much less when measured in rotation periods since a rotation period for these two cases is about 13 years.

After a short adjustment period, the models maintain statistically steady solutions. For example, figure 1 shows the total kinetic and magnetic energies over a portion of the simulation for case 1.

### 3. Results

In general, the difference in Prandtl number appears to have a greater effect on the magnetic field produced than the addition of a plausible amount of radiogenic heating. Here we show results comparing the magnetic fields produced by all five simulations with greater analysis for the new cases 1 and 2.

### 3.1. Kinetic and magnetic energies

The total kinetic energy of case 2 is consistently 10–20% smaller than that of case 1. The higher kinetic energy of case 1 is probably due to the difference in heat source distribution between the two cases. Case 1 has its source of buoyancy (thermal and compositional) mainly at the inner core boundary; whereas case 2 has some internal heating distributed throughout the core, and therefore smaller heat and compositional fluxes at the inner core boundary. The greater inner boundary buoyancy source of case 1 is much more effective at driving convection than the volumetric heating of case 2 because of the greater gravitational potential for the former and the additional compositional buoyancy source proportional to the latent heat flux as the inner core grows. This effect can be seen in the upwellings and downwellings which are both typically stronger in case 1 than in case 2 (figure 3).

Since more latent heat and light constituents are released at the inner core boundary for case 1, the rate of change of the radius of the inner core (Glatzmaier and Roberts 1996a) exceeds that of the radiogenic case. The rate for case 1 is typically about 400m/Myr and that for case 2 is about 300m/Myr, which suggests a significantly older inner core for case 2.

The fluid flow patterns of cases 1 and 2 are qualitatively very similar. (Fluid flow is considered relative to the rotating frame of reference, which is the frame in which the total angular momentum of the model planet is equal to zero.) In both cases, the average longitudinal flow is westward near the CMB. The average longitudinal flow at higher latitudes near the inner core boundary is eastward, as is the average rotation rate of the solid inner core.

For cases 1 and 2, the amplitude of the maximum convective velocity (about  $10^{-3} \text{ ms}^{-1}$ ) is roughly what is expected for the Earth's core, but the magnetic field intensity is about 30 times smaller than that of the Earth (figure 4). However, the Elsasser number ( $\Lambda_E$ ) for cases 1 and 2 (tables 2 and 3) is within an order of magnitude of the Earth's Elsasser number because of the much slower rotation rate in these simulated cases. Cases 3–5 have similar convective velocity amplitudes, but a more Earth-like magnetic field intensity (figure 4).

Cases 1 and 2 have qualitatively similar magnetic field structures within the core and at the CMB. There is a dominantly dipolar field structure at the CMB and a more complicated structure within the core. Snapshots of the magnetic field in these two cases are seen in figure 2 where the magnetic field is plotted as field lines (a) and as radial magnetic field at the CMB (b). The dominance of the dipolar structure at and above the CMB is clearly seen. Despite the similarities in the structure of the magnetic field within the core, the total magnetic energies of the two cases differ. Case 2 consistently has 10–20% greater total magnetic energy than that of case 1. Apparently, in this parameter regime (i.e. smaller rotation rate and Coriolis forces), the stronger convection of case 1 results in weaker shear and helical flows, and hence lesser magnetic induction. (For a comparison of models with different rotation rates, see Kono and Roberts 2002.)

Due to the large magnetic Prandtl number ( $P_m$ ) of cases 3–5, the magnetic energy in these cases is about three orders of magnitude higher than the kinetic energy (Glatzmaier and Roberts 1995, Simitev and Busse 2005), which is what is expected for the Earth based on the intensity and the secular variation of the geomagnetic field. With  $P_m = 1$  in cases 1 and 2, the difference in magnitudes of the kinetic and

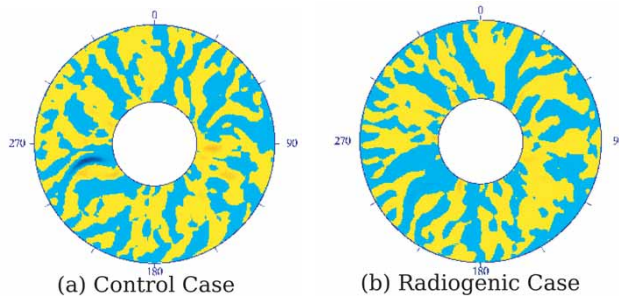


Figure 2. Snapshots of radial velocity for cases 1 and 2 in the equatorial plane. The golden (lighter) color denotes the radially outward velocities, the blue (darker) color denotes the radially inward. Case 1 shows stronger upwellings and downwellings than case 2.

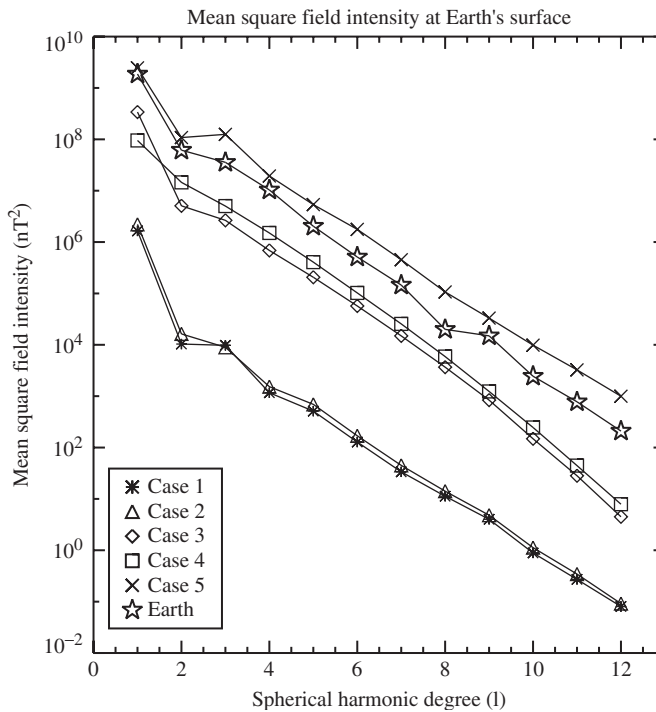


Figure 3. Mean square field intensity at surface versus spherical harmonic degree ( $l$ ) for Earth (Glatzmaier and Roberts, 1996b) and simulated cases (table 1).

magnetic energies in figure 1 is much less. For case 1, the mean value over time of the total volume integrated magnetic energy is only about 2.4 times that of the kinetic energy. This smaller difference is due to the smaller dominance of Coriolis forces relative to buoyancy forces in case 1, which results in less shear and helicity and therefore a lesser magnetic induction compared to cases 3–5. The convective Rossby number ( $Ro_c$ , table 2), which is an estimate of the ratio of the buoyancy to Coriolis forces (Glatzmaier 2005 and

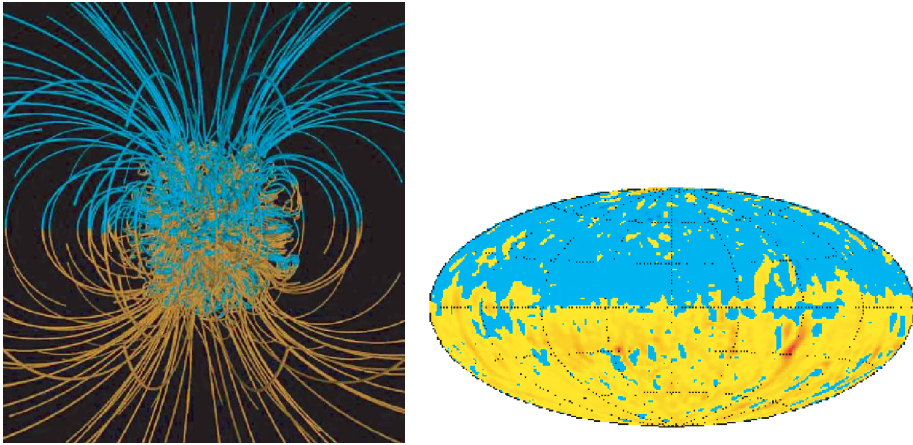


Figure 4. Snapshot of magnetic field for case 1. (a) Magnetic field lines – gold represents the outgoing field, blue indicates the inward directed field. (b) Radial magnetic field at the CMB – red and gold represent the outward directed field, and blue inward field. Both the figures show a dipole-dominant magnetic field structure.

Christensen 2002), is about 25 times greater for cases 1 and 2 compared with cases 3–5 (table 3).

### 3.2. Magnetic energy spectra at the Earth's surface

Figure 4 shows the magnetic energies (field intensity squared) per spherical harmonic degree for the five cases and the Earth to degree 12. The magnetic energy per degree for cases 1 and 2 are two to three orders of magnitude lower than those for the Earth and cases 3–5 (Coe *et al.* 2000). In addition to the magnitude of the spectra, the dipole is also more dominant in cases 1 and 2 than in cases 3–5 and the Earth. Cases 3–5 use the same magnetic diffusivity and have the same convective velocity amplitudes as cases 1 and 2. However, the rotation rate for cases 3–5 is set to that of the Earth producing stronger Coriolis forces than those in cases 1 and 2. Clearly, the magnitude of the Coriolis force significantly affects the intensity and spectral content of the simulated fields.

There is a slight difference between cases 1 and 2 in their quadrupole ( $l=2$ ) and octupole ( $l=3$ ) terms. Case 2 and the Earth have a quadrupole that is greater than the octupole. Case 1 has an octupole that is greater than the quadrupole. At a first glance, it appears as though case 2 is more “Earth-like” than case 1 in this respect. However, the data plotted here are time averages of the simulated cases and only a snapshot of the Earth’s present day field. Case 2 does not always have a larger quadrupole than octupole, and case 1 sometimes shows a smaller octupole. It is impossible to constrain the average octupole/quadrupole relationship for the Earth over long times because of the lack of sufficient data. Therefore, one cannot use the octupole/quadrupole relationship in our simulations as evidence for or against the radiogenic heating in the core.

In addition to having a magnetic Prandtl number of unity, cases 1 and 2 also differ from the other cases because they do not include hyperdiffusivity. Case 5 has a large

magnetic Prandtl number of the same order of magnitude as the previous simulations (cases 3 and 4), but only a minute amount of hyperdiffusivity. The large amount of hyperdiffusion employed in cases 3 and 4 causes the energy to decrease somewhat faster with spherical harmonic degree compared with the other three cases and the Earth, as can be seen in figure 4 starting at about degree 7. The higher resolution and much lower hyperdiffusion of case 5 results in magnetic energies about an order of magnitude greater than those of cases 3 and 4.

### 3.3. *Paleosecular variation*

Virtual geomagnetic poles (VGPs) are calculated from sampling locations at every 10 degrees longitude for every 10 degrees latitude roughly every model day. In order to analyze the secular variation of our simulations, angular standard deviation (ASD) of these VGPs is calculated for each 10 degrees of latitude using  $ASD = (\sum_{i=1}^N \theta_i^2 / (N - 1))^{1/2}$  where  $N$  is the number of samples, and  $\theta_i$  is the angular deviation from the geographic pole of the  $i$ th VGP. To correct for the bias due to excursions and pole reversals, we use the accepted method of Vandamme (1994) which applies a recursive method to determine the optimum cutoff angle for exclusion of VGP data.

Figure 5 shows the calculated angular ASDs for the simulated cases and the Earth. None of the simulations shows the large increase in ASD with latitude that is seen in the Earth data. For three of the cases (1–3), the magnetic field produced is more stable than that of the Earth for all latitudes. Cases 1 and 2 have small ASD because of the small relative effects of the Coriolis force, as discussed above. These two cases also show an increase in ASD with latitude, which is also seen in the profile for the Earth and other models with Prandtl numbers of unity (Kono and Roberts 2002). The small ASD for case 3 is likely due to the homogeneous heat flux boundary condition at the CMB (Glatzmaier *et al.* 1999). For case 4, which has a tomographic CMB heat flux boundary condition but low spatial resolution and case 5, which has a homogeneous CMB heat flux boundary condition, higher spatial resolution, and a higher magnetic Reynolds number (table 1), the fields are less stable than the Earth at low latitudes, but are more stable at higher latitudes. However, their global standard deviations are similar to that of the Earth.

### 3.4. *Transient feature*

For cases 1 and 2, a transient magnetic field structure at the geographic poles appears intermittently in both cases (figure 6). A strong concentration of radial magnetic field is sometimes seen in one of the polar regions, centered at roughly half the core radius. When a field intensification like this occurs, the magnetic field line plots (figure 6) often show “vortex” field structures coincident with strong fluid vortex. This feature appears on-and-off at different times in both cases and persists, on average, about 500 model years. Usually, this feature does not occur at both geographic poles at the same time. A similar feature, although not intermittent, has also been seen in the geodynamo simulations of Sreenivasan and Jones (2005).

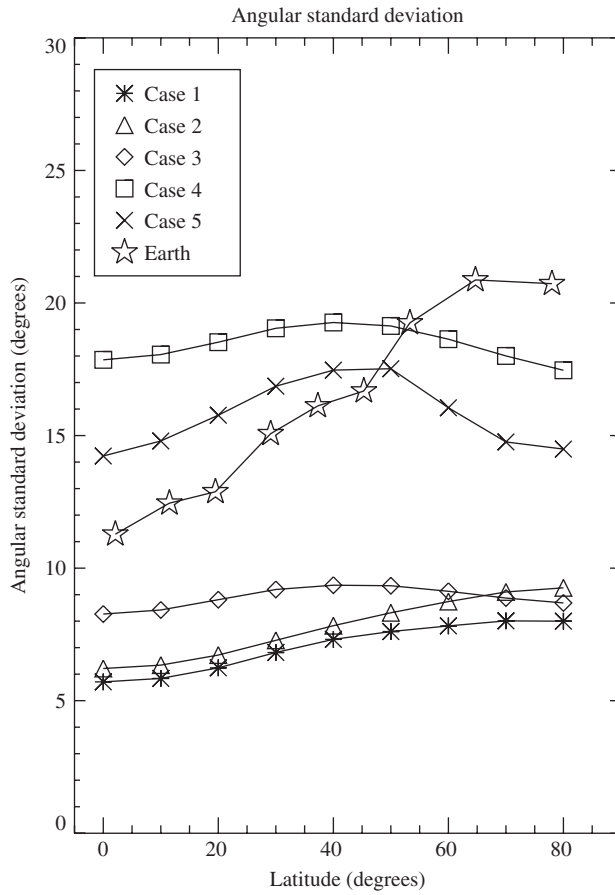


Figure 5. Angular standard deviation of the virtual geomagnetic poles for Earth (McElhinny and McFadden 1997) and simulated cases (table 1). Calculation and cutoff angle method from Vandamme (1994).

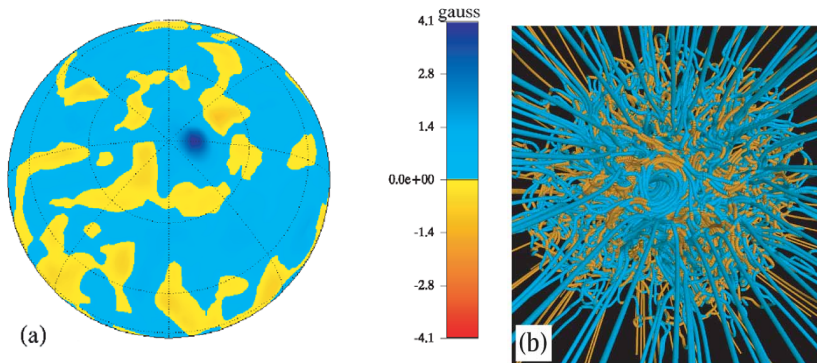


Figure 6. Transient field structure, north pole view for case 1. (a) Radial magnetic field at mid-depth in the FOC. (b) Magnetic field lines. The golden color represents the outward field, and blue represents the inward field.

#### 4. Discussion

In order to compare geodynamo simulations with field data, it is necessary to have an appropriate measure of the Earth's field, with which to compare the simulation results. The geodynamo models provide a complete spatial data coverage over the simulation's entire duration. This is limited only by the spatial resolution chosen and the frequency with which data is saved. Obtaining reliable time-averages for the Earth's field has far greater limitations. Researchers still debate the number of years needed to obtain a robust time-averaged field for the Earth and how accurately the structure of the time averaged field is known (Gubbins and Kelly 1993, McElhinny *et al.* 1996, Carlot *et al.* 1999). It is important to keep these caveats in mind as we compare the geodynamo model field results with the Earth's palaeomagnetic surface field.

Internal heating has been tested as a power source in previous geodynamo simulations. One of the cases examined by Kutzner and Christensen (2000) powered totally by internal heating produces a dominantly quadrupolar or more complex field with an irregular distribution of magnetic flux spots of either polarity in both hemispheres. However, a strong dipolar magnetic field can be produced with only internal heating if the inner core is removed (Sakuraba and Kono 1999) or is much smaller than its present day size (Roberts and Glatzmaier 2001). A later study by Kutzner and Christensen (2002) compared a greater variety of driving mechanisms for the geodynamo including three cases with different levels of internal heating (10, 50, and 100% of the superadiabatic heat flow). They produce the dipole-dominated magnetic fields at the model surface for their 10% internal heating cases, but not for their 50 and 100% internal heating cases, which were dominated by smaller scale magnetic field structures. Although the 25% internally heated case we present here also produces a dipole-dominated field at the model surface, it is difficult to compare our model results with those of Kutzner and Christensen (2000, 2002) because our model accounts for density stratification and compositional buoyancy, has different thermal and magnetic boundary conditions, and is run at higher spatial resolution with different parameter specifications.

#### 5. Conclusions

The first objective of this study was to identify the major effects on a geodynamo simulation due to changes in various parameters while maintaining comparable, Earth-like convective velocity amplitudes. Compared with previously published simulations produced with the Glatzmaier–Roberts model, two of the new simulations presented here (cases 1 and 2) have all diffusivities set equal (as most other geodynamo models have prescribed) instead of having a much greater viscous diffusivity (as in previous Glatzmaier–Roberts simulations). The price paid for this is a rotation rate much less than that of the Earth's (because of the limitation on the Ekman number) and a much smaller superadiabatic heat flow (because of the limitation on the Rayleigh number). As a result, the Coriolis forces are less dominant over the buoyancy forces, and therefore the generated magnetic field is much less intense and less variable than the high magnetic Prandtl number simulations of Glatzmaier and Roberts (cases 3 and 4) and the new higher resolution case 5.

The second goal of this study was to compare the results of two geodynamo simulation cases (1 and 2), one with and one without the radiogenic heating in the core. The hope was that one would appear more “Earth-like,” thus supporting or refuting the suggestion that there is radiogenic heating in the Earth’s core. The total superadiabatic heat flux through the CMB is made the same for both cases. The inner core for the radiogenic case grows three-quarters as fast in radius. Although the generated magnetic fields for these two cases are quite similar, there are some differences between the two cases – their average total kinetic and magnetic energies, the time-average relationship between the octupole and quadrupole, and the ASDs of their virtual geomagnetic poles – but these are insufficient to determine which case is more “Earth-like.” From this study, it is possible to say that the radiogenic potassium may be present in the core as its addition to the geodynamo model does not make the field any less “Earth-like.” However, there is no robust evidence here to support the idea that it must be – or even probably is – present in the core.

### Acknowledgment

Support for this research was provided by NSF (EAR-0221941) and IGPP (at UCSC and LANL). Computing resources were provided by the Pittsburgh Supercomputing Center and NSF/MRI (AST-0079757). The authors would like to thank the two referees for the helpful suggestions.

### References

- Brodholt, J. and Nimmo, F., Core values. *Nature*, 2002, **418**, 489–491.
- Buffett, B., Estimates of heat flow in the deep mantle based on the power requirements of the geodynamo. *Geophys. Res. Lett.*, 2002, **29**, 1566–1570.
- Busse, F.H., Homogeneous dynamos in planetary cores and in the laboratory. *Ann. Rev. Fluid Mech.*, 2000, **32**, 383–408.
- Busse, F.H., Convective flows in rapidly rotating spheres and their dynamo action. *Phys. Fluids*, 2002, **14**, 1301–1314.
- Carlut, J., Courtillot, V. and Hulot, G., Over how much time should the geomagnetic field be averaged to obtain the mean paleomagnetic field? *Terra Nova*, 1999, **11**, 239–243.
- Chabot, N.L. and Drake, M.J., Potassium solubility in metal: the effects of composition at 15 kbar and 1900°C on partitioning between iron alloys and silicate melts. *Earth Planet. Sci. Lett.*, 1999, **172**, 323–335.
- Christensen, U., Zonal flow driven by strongly supercritical convection in rotating spherical shells. *J. Fluid Mech.*, 2002, **470**, 125–133.
- Christensen, U., Aubert, J., Cardin, P., Dormy, E., Gibbons, S., *et al.*, A numerical dynamo benchmark. *Phys. Earth Planet. Inter.*, 2001, **128**, 25–34.
- Coe, R.S., Hongre, L. and Glatzmaier, G.A., An examination of simulated geomagnetic reversals from a palaeomagnetic perspective. *Phil. Trans. Roy. Soc.*, 2000, **358**, 1141–1170.
- Dormy, E., Valet, J.-P. and Courtillot, V., Numerical models of the geodynamo and observational constraints. *Geochem. Geophys. Geosyst.*, 2000, **1**.
- Fearn, D.R., Hydromagnetic flow in planetary cores. *Rep. Prog. Phys.*, 1998, **61**, 175–235.
- Gessman, C.K. and Wood, B.J., Potassium in the Earth’s core? *Earth Planet. Sci. Lett.*, 2002, **200**, 63–78.
- Glatzmaier, G.A., Numerical simulations of stellar convective dynamos. I. The model and method. *J. Comp. Phys.*, 1984, **55**, 461–484.
- Glatzmaier, G.A., Geodynamo simulations – How realistic are they? *Ann. Rev. Earth Planet. Sci.*, 2002, **30**, 237–257.

- Glatzmaier, G.A., Planetary and stellar dynamos: challenges for next generation models. In: *Fluid Dynamics and Dynamos in Atmospherics and Geophysics*, A.M. Soward, C. Jones, D. Hughes, N. Weiss (Eds), 2005 (CRC Press: London), 331–357.
- Glatzmaier, G.A., Coe, R.S., Hongre, L. and Roberts, P.H., The role of the Earth's mantle in controlling the frequency of geomagnetic reversals. *Nature*, 1999, **401**, 885–980.
- Glatzmaier, G.A. and Roberts, P.H., A three-dimensional convective dynamo solution with rotating and finitely conducting inner core and mantle. *Phys. Earth Planet. Inter.*, 1995, **91**, 63–75.
- Glatzmaier, G.A. and Roberts, P.H., An anelastic evolutionary geodynamo simulation driven by compositional and thermal convection. *Physica D*, 1996a, **97**, 81–94.
- Glatzmaier, G.A. and Roberts, P.H., On the magnetic sounding of planetary interiors. *Phys. Earth Planet. Inter.*, 1996b, **98**, 207–220.
- Glatzmaier, G.A. and Roberts, P.H., Simulating the Geodynamo. *Contemp. Phys.*, 1997, **38**, 269–288.
- Gubbins, D. and Kelly, P., Persistent patterns in the geomagnetic field over the past 2.5 Myr. *Nature*, 1993, **365**, 829–832.
- Kageyama, A. and Sato, T., Computer simulations of a magnetohydrodynamic dynamo II. *Phys. Plasmas*, 1995, **2**, 1421–1431.
- Kono, M. and Roberts, P.H., Recent geodynamo simulations and observations of the geomagnetic field. *Rev. Geophys.*, 2002, **40**, 41–53.
- Kutzner, C. and Christensen, U., Effects of driving mechanisms in geodynamo models. *Geophys. Res. Lett.*, 2000, **27**, 29–32.
- Kutzner, C. and Christensen, U., From stable dipolar towards reversing numerical dynamos. *Phys. Earth Planet. Inter.*, 2002, **131**, 29–45.
- McElhinny, M.W., McFadden, P.L. and Merrill, R.T., The time-averaged paleomagnetic field 05 Ma. *J. Geophys. Res.*, 1996, **101**, 25,007–25,027.
- McElhinny, M.W. and McFadden, P.L., Paleosecular variation over the past 5 Myr based on a new generalized database. *Geophys. J. Int.*, 1997, **131**, 240–252.
- Murthy, V.R., van Westrenen, W. and Fei, Y., Experimental evidence that potassium is a substantial radioactive heat source in planetary cores. *Nature*, 2003, **423**, 163–165.
- Nimmo, F., Price, G.D., Brodholt, J. and Gubbins, D., The influence of potassium on the core and geodynamo evolution. *Geophys. J. Int.*, 2004, **156**, 263–276.
- Ohtani, E., Yurimoto, H. and Seto, S., Element partitioning between liquid, silicate liquid, and lower-mantle minerals: implications for core formation of the Earth. *Phys. Earth Planet. Inter.*, 1997, **100**, 92–114.
- Parker, L.J., Atou, T. and Badding, J.V., Transition element-like chemistry for potassium under pressure. *Science*, 1996, **273**, 95–97.
- Roberts, P.H. and Glatzmaier, G.A., Geodynamo theory and simulations. *Rev. Mod. Phys.*, 2000, **72**, 1081–1123.
- Roberts, P.H. and Glatzmaier, G.A., The geodynamo, past, present, and future. *Geophys. Astrophys. Fluid Dyn.*, 2001, **94**, 47–84.
- Sakuraba, A. and Kono, M., Effect of the inner core on the numerical solution of the magnetohydrodynamic dynamo. *Phys. Earth Planet. Inter.*, 1999, **111**, 105–121.
- Simitev, R. and Busse, F.H., Prandtl number dependence of convection-driven dynamos in rotating spherical fluid shells. *J. Fluid Mech.*, 2005, **532**, 365–388.
- Sreenivasan, B. and Jones, C.A., Structure and dynamics of the polar vortex in the Earth's core. *Geophys. Res. Lett.*, 2005, **32**.
- Stacey, F.D., *Physics of the Earth*, 1992 (Brookfield Press: Brisbane).
- Vandamme, D., A new method to determine paleosecular variation. *Phys. Earth Planet. Inter.*, 1994, **85**, 131–142.